ResearchGate

See discussions, stats, and author profiles for this publication at: https://www.researchgate.net/publication/231653504

# Enhanced Efficiency of Organic Dye−Sensitized Solar Cells: Triphenylamine Derivatives

**ARTICLE** *in* THE JOURNAL OF PHYSICAL CHEMISTRY C · SEPTEMBER 2009

Impact Factor: 4.77 · DOI: 10.1021/jp904946a

CITATIONS
133

READS
278

**4 AUTHORS**, INCLUDING:

Catherine Michaux
University of Namur
**87** PUBLICATIONS **1,788** CITATIONS
SEE PROFILE

Denis Jacquemin
University of Nantes
**356** PUBLICATIONS **8,276** CITATIONS
SEE PROFILE

Eric A Perpète
University of Namur
**173** PUBLICATIONS **6,026** CITATIONS
SEE PROFILE

Available from: Denis Jacquemin
Retrieved on: 01 February 2016

# Enhanced Efficiency of Organic Dye-Sensitized Solar Cells: Triphenylamine Derivatives

**Julien Preat,*,†,§ Catherine Michaux,‡,|| Denis Jacquemin,†,⊥ and Eric A. Perpète†,▽**

*Laboratoire de Chimie Théorique Appliquée, Facultés Universitaires Notre-Dame de la Paix, rue de Bruxelles, 61, 5000 Namur, Belgium, and Laboratoire de Chimie Biologique Structurale, Facultés Universitaires Notre-Dame de la Paix, rue de Bruxelles, 61, 5000 Namur, Belgium*

*Received: May 27, 2009; Revised Manuscript Received: July 15, 2009*

A general TDDFT procedure has been set up that accurately evaluates the UV/vis absorption spectra of a series of new conjugated metal-free organic dyes based on the triphenylamine (TPA) moiety, which have recently been developed for dye-sensitized solar cells (DSSCs). It turns out that the BHandH functional, combined with the 6-311+G(2d,2p) basis set, gives reliable auxochromic shifts when the bulk solvation effects are included in the model. Indeed, the theoretical procedure provides $\lambda_{max}$ with a mean absolute deviation limited to ~0.1 eV only. In addition, we give insights into the geometrical and electronic structures of the dyes, and we unravel the structural modifications allowing to optimize the properties of TPA-based DSSCs. This investigation aims at improving the electron-injection process, as well as the light-harvesting efficiency (LHE) of the dyes. To this purpose, we considered a set of about 20 new dyes, and starting from the TPC-1 structure, the following modifications help to get better electron injection and light-harvesting properties: (i) the extension of the bridging group by addition of an ethylene subunit between the two phenyl groups (TPC-14); (ii) the 16-COOH, 15-OMe, 1a,6-diCN functionalization (TPC-18); (iii) moving the terminal cyano acceptor from the 16 to the 15 position, while introducing two −OMe functions in 11 and 13 positions and/or grafting two −CN groups in 1a and 6 positions on the TPA moiety (TPC-20). These specific modifications induce a maximal increase of the LHE and a more exoenergic free enthalpy of injection (−2.20 eV compared to −1.84 eV for TPC-1). Finally, TPC-23 (which results from the TPC-14/TPC-20 combination) shows an improvement of both the spectroscopic and energetic parameters. Moreover, the molecular topology analysis demonstrates that the coplanarity between the anchoring and the bridging unit is broken, that is, the positive charge is not directly in contact with the $TiO_2$ surface, and the recombination reaction is therefore inhibited.

## Introduction

The present energetic and environmental crisis has stimulated the interest in the design of renewable energy sources. In this field, dye-sensitized solar cells (DSSCs) certainly appear as one of the most promising devices for converting the solar energy and have therefore attracted significant attention as low-cost alternatives to conventional semiconductor (SC) photovoltaic devices. These cells are composed of a wide band gap semiconductor (like $TiO_2$) deposited on a translucid conducting substrate, an anchored molecular sensitizer, and a redox electrolyte (the $I^-/I_3^-$ couple).[1−5]

The Ru complexes photosensitizers such as the N3 and N719 compounds [*cis*-di(thiocyanato)-bis(2,2′-bipyridyl-4,4′-dicarboxylate) ruthenium(II)] show a solar energy-to-electricity conversion efficiency of 10% on average. Nevertheless, an increasing interest for purely organic DSSCs as the substitutes for Ru complexes raised in recent years due to crucial advantages such as the high molar extinction coefficient, simple and relatively inexpensive preparation processes, and compliance with environmental and health issues.[6] Moreover, the solid-state DSSCs based on organic dyes show better performances than ruthenium complexes, and that suggests promising commercial applications featuring these organic dyes.[7] Therefore, metal-free dyes like coumarin,[8] merocyanine,[9] indoline,[10] xanthene,[11] hemicyanine,[12] perylene, and fluorene[13,14] are good potential candidates to build DSCCs.

The basic structure of most of the organic sensitizers is made of a donor (D), a bridge (B, typically a $\pi$ spacer), and an acceptor (A) moieties, which are usually combined following a D-$\pi$-A rodlike configuration (Scheme 1) in order to improve the efficiency of the UV/vis photoinduced intramolecular charge transfer (ICT). Generally, the critical factors that influence the sensitization are (i) the excited-state redox potential has to match the energy of the conduction band (CB) edge of the semiconductor; (ii) the highest occupied molecular orbital (HOMO) must fit the iodine/iodide redox potential, and the lowest unoccupied molecular orbital (LUMO) has to be higher in energy than the conduction band edge of the semiconductor; (iii) a huge light-harvesting ability of the dye is crucial to get a substantial photocurrent response; (iv) the good conjugation across the donor and anchoring group determines the large charge transfer (CT) character of the electronic transition; (v) the electronic coupling strength between dye's LUMO and the semiconductor CB is of course a key property for an efficient electron injection from the dye onto the semiconductor surface. Note that in general, the major factors leading to a low conversion efficiency of many organic dyes in DSSC are the formation of dye

* To whom correspondence should be addressed. E-mail: julien.preat@fundp.ac.be.
† Laboratoire de Chimie Théorique Appliquée.
‡ Laboratoire de Chimie Biologique Structurale.
§ Postdoctoral Researcher of the Belgian National Fund for Scientific Research.
|| Postdoctoral Researcher of the Belgian National Fund for Scientific Research.
⊥ Research Associate of the Belgian National Fund for Scientific Research.
▽ Senior Research Associate of the Belgian National Fund for Scientific Research.

10.1021/jp904946a CCC: $40.75 © 2009 American Chemical Society
Published on Web 08/31/2009

**SCHEME 1: Sketch of a Typical D-B-A System Used As Dye-Sensitizer**

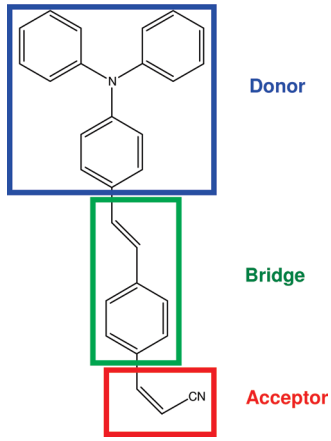


aggregates and charge recombination between the CB electrons and the dye$^+$ or the electrolyte.[15−17]

To further design and develop more efficient metal-free dyes for DSSCs, appropriate DBA systems are needed whose properties can be finely tuned by applying the adequate structural modifications. Recently, it has been found that triphenylamine (TPA)-like moieties and a cyanoacetic acid group are units of choice as electron donor and electron acceptor/anchoring groups, respectively.[15,18] Indeed, the TPA moiety is expected to greatly confine the cationic charge from the semiconductor surface and efficiently hamper the recombination. TPA also shows a huge steric hindrance and can therefore prevent unfavorable dye aggregation at the semiconductor surface.[18]

The bridging groups guide light absorption regions of the DSSCs and subsequently the scale of the electron injection from the excited state of the dyes to the semiconductor surface. Accordingly, we will herein report on the design of new molecules derived from the several organic dyes recently synthetized by Haining Tian et al.[19] and Wei Xu et al.[20] More precisely, the investigated dyes consist of a TPA connected to the acceptor (cyanoacetic acid or rhodanine-3-acetic acid) moiety by phenylene (the bridging $\pi$-spacer). We also consider similar systems in which the bridging phenylene group has been replaced by a furan that, due to its smaller resonance energy (16 kcal·mol$^{-1}$ compared to 36 kcal·mol$^{-1}$ for the benzene), provides a more effective conjugation and lowers the energy of the photoinduced charge transfer.[21]

Currently, molecular modeling techniques and especially quantum chemistry (QM) offer a competitive alternative for the interpretation of the experimental data arising from industrial interests and developments. The improvements in CPU resources now allow the study, at correlated levels of approximation, of the absorption spectra of large molecular species such as the DSSCs dyes. For UV/vis calculations, one of the most popular approach remains time-dependent density functional theory (TDDFT), which commonly provides accurate results for a reasonable computational effort, especially when hybrid functionals are used.[22−29] It is well known that "cyanine-like" structures, such as TPA derivatives, show large CT-character electronic excitations (sometimes with a multideterminental nature) which make them difficult to study with DFT (the last one tends to overestimate CT effects). The "long-range corrected" functional, especially tailored for CT systems, could reduce the error in many cases[30−35] but apparently not for cyanine systems.[36] Still, the use of conventional DFT approaches to compute auxochromic shifts for CT dyes is not uncommon in literature.[37−39]

Therefore, we have set up a general TDDFT-based theoretical procedure for the UV/vis prediction of TPA absorption spectra, and we strive for the 0.1−0.2 eV accuracy that is the generally accepted upper limit required for the design of new industrial dyes. To meet this target, our computational procedure is taking into account the solvation process of the dyes by means of the polarizable continuum model (PCM).[40,41] This above-mentionned procedure is also used to gain insights into the geometrical and electronic structures, of the dyes and to bring up the adequate structural modifications to optimize the properties of the TPA-based DSSCs. More precisely, in this contribution, we focus on the free energy of the electron injection onto the $TiO_2$ substrate and on the light harvesting abilities of the dyes.

## Methodology

**Computational Aspects.** All calculations have been performed with the Gaussian 03 package,[42] following a two-step procedure: (i) the optimization of the ground state geometry with DFT or within the second-order Møller−Plesset (MP2) theory[43] and (ii) the determination of the vertical electronic excitation energies by means of TDDFT. Several Pople basis sets (BSs) have been tested−6-31G(d,p), 6-31+G(d,p), 6-311G(d,p), 6-31G(2d,2p), 6-311G(2d,2p), and 6-311G(2df,2pd). For the TDDFT calculations, we also considered additional 6-311G+(2d,2p) and 6-311G+(2df,2pd) BSs.[44] The geometry optimizations have been performed with a *tight* threshold, that corresponds to rms (residual mean square) residual forces smaller than $10^{-5}$ a.u. for the optimal geometry. Following each optimization, the vibrational spectrum has been determined, and it has systematically been checked that all vibrational frequencies are real.

For the first step, we have used the popular three-parameter B3LYP functional,[45] in which the exchange is a combination of 20% Hartree−Fock (exact) exchange, Slater functional, and Becke's generalized gradient approximation (GGA) correction,[46] whereas the correlation part combines local and Lee−Yang−Parr (LYP) functionals.[47] For the TDDFT calculations, we used three extra functionals: (i) the BHandH hybrid designed by Becke with 50% of LSDA exchange,[48] (ii) the parameter-free PBE0 hybrid functional that is built on the Perdew−Burke−Ernzerhof pure functional, in which the exchange is weighted (75% DFT/25% HF) according to theoretical considerations and[49−52] (iii) the three-parameter O3LYP functional, which is similar to B3LYP but contains only 11.61% of exact exchange and a GGA correction based upon the OPTX functional.[53]

All the theoretical $\lambda_{max}$ reported in the following correspond to the first singlet excited state with dipole-allowed transitions (i.e., nonzero oscillator strength *f*) from the ground state. The iodine/iodide couple is used as regenerator of the DCCS, and this implies that the solar cells work in solvent phase. This is why the UV/vis experimental data for TPA-based dyes are reported in solution and the PCM[25,40,41] is used for evaluating bulk solvent effects. In PCM, one usually divides the problem into a solute part (the dye) lying inside a cavity and a solvent part. By solving Poisson's equation at the interface, PCM is able to return a valid approximation of solvent effects as long as no solute−solvent specific interactions do not exist. We have selected the so-called nonequilibrium PCM solutions, and we refer the reader to ref 25 for extensive details about this procedure.

**Setting up the Procedure.** On the basis of electron diffraction patterns and in combination with ab initio calculations, Naumov et al.[54] have shown in a recent study that the unsubstituted TPA moiety pertains to the $C_3$ group, and we therefore kept a similar

**TABLE 1: Indirect BS Effects in nm [in eV] on the UV/Vis Absorption Spectrum of TPA-m[a]**

| | TDB3LYP/6-31G(d,p)//B3LYP/X | | | | | | |
|---|---|---|---|---|---|---|---|
| X | 6-31G(d,p) | 6-31G(2d,2p) | 6-311G(d,p) | 6-311G(2d,2p) | 6-311G(2df,2pd) | 6-31+G(d,p) | MP2/6-31G(d,p) |
| $\lambda_{max}^{(1)}$ | 478 [2.60] | 476 [2.60] | 474 [2.62] | 472 [2.63] | 472 [2.63] | 478 [2.59] | 470 [2.64] |
| $\lambda_{max}^{(2)}$ | 350 [3.54] | 349 [3.56] | 347 [3.57] | 346 [3.59] | 346 [3.59] | 350 [3.54] | 346 [3.59] |
| $d_{C1c-N}$ | 1.413 | 1.409 | 1.412 | 1.410 | 1.408 | 1.413 | 1.407 |
| $d_{C4-N}$ | 1.425 | 1.422 | 1.424 | 1.423 | 1.421 | 1.425 | 1.415 |
| $d_{C15-C16}$ | 1.352 | 1.349 | 1.349 | 1.346 | 1.345 | 1.354 | 1.351 |
| $\alpha_{C14-C9-C8-C7}$ | | | | 180.00 | | | 157.00 |

[a] The reference geometry is MP2. For all the B3LYP structures, several geometrical parameters (C−N and C−C bond lengths in Å; α dihedral angle in degrees) are compared with MP2 results.

**TABLE 2: Direct BS Effects in nm [in eV] on the UV/Vis Absorption Spectrum of TPA-m**

| | TDB3LYP/X//B3LYP/6-31G(d,p) | | | | | | |
|---|---|---|---|---|---|---|---|
| X | 6-31G(d,p) | 6-31G(2d,2p) | 6-311G(d,p) | 6-311G(2d,2p) | 6-311G(2df,2pd) | 6-311+G(2d,2p) | 6-311+G(2df,2pd) |
| $\lambda_{max}^{(1)}$ | 478 [2.60] | 478 [2.60] | 484 [2.56] | 484 [2.56] | 484 [2.57] | 494 [2.51] | 493 [2.52] |
| $\lambda_{max}^{(2)}$ | 350 [3.54] | 350 [3.54] | 355 [3.50] | 355 [3.49] | 355 [3.49] | 362 [3.42] | 362 [3.43] |

conformation for all the studied derivatives. The prototype molecules used for this methodological stage is TPA-m (see Scheme 1). The establishment of an efficient computational framework highly depends on the appropriate choice of BSs and functionals. As a starting procedure, B3LYP is selected for the ground-state optimizations, as well as for the TDDFT calculations. Tables 1 and 2 show both the indirect (a modification of the ground-state geometry) and the direct (a perturbation of the excitation spectrum) basis set effects on the excitation energy (in nm) of TPA-m. It turns out that 6-31G(d,p) is a satisfying BS for the geometry optimization, as there are no significant changes in the $\lambda_{max}$ values (∼3 nm in average) when additional polarization, diffuse, or valence functions are included. Moreover, the agreement between the spectra evaluated using B3LYP and MP2 structures is excellent, the differences being limited to 5 nm. In addition, we also compare in Table 1 some of the representative geometrical parameters of the TPA-m chromophoric unit. On the electron-donor side, we probe the $d_{C1c-N}$ (see Scheme 2) and $d_{C4a-N}$ (or $d_{C1c-N}$) bond lengths, whereas in the acceptor zone, the $d_{C15-C16}$ and the bridging $\alpha_{C14-C9-C8-C7}$ dihedral angle (in degrees) are investigated. It turns out that the B3LYP bond lengths do not depend upon the BS and are almost identical to the MP2 values. Indeed at the B3LYP/6-31G(d,p) level, the $d_{C1c-N}$, $d_{C4a-N}$, and $d_{C15-C16}$ are 1.41, 1.43, and 1.35 Å, respectively, whereas the MP2 parameters are 1.41, 1.42, and 1.35 Å. Only the bridging dihedral angle (α) differs in the DFT framework, the TPA-m is planar, while with MP2 the coplanarity is broken (∼25° out-of-plane distortion), resulting in a shift of the entire UV/vis spectrum ($\lambda_{max}^{(1)}-\lambda_{max}^{(2)}$) to the lower wavelengths (higher energies).

Thus, we validate B3LYP for optimizing the geometry, as it provides results close to MP2, at a much smaller computational cost. On the other side, the visible spectra are much more sensitive to the BS extension, that is, ∼15 nm when extra polarization, valence, and diffuse functions are simultaneously added. As a compromise between accuracy and basis set size, we have opted for 6-311G+(2d,2p) for the TDDFT calculations, bearing in mind that extra d and f functions would only lead to negligible refinements. To estimate transition energies, using larger BSs than for ground-state geometries optimization is not uncommon: for most of conjugated compounds, the excitation process often induces a charge separation (that actually needs extended BSs) at the chromophore level, and the weight of these zwitterionic-like structures is generally larger in the excited state of polar molecules.

For most of the investigated compounds, we have found in the UV/vis region two allowed excited states, characterized by large transition probabilities. This is in complete agreement with the experimental findings, since most measurements show a intense first absorption band [$\lambda_{max}^{(1)}$] in the 400−600 nm region, and a second absorption band [$\lambda_{max}^{(2)}$] of high intensity in the 300 nm region. $\lambda_{max}^{(1)}$ and $\lambda_{max}^{(2)}$ are associated to excitations predominantly implying three molecular orbitals: HOMO → LUMO for $\lambda_{max}^{(1)}$ and HOMO-1 → LUMO for $\lambda_{max}^{(2)}$. As can be seen in Figure 1, for TPC-1 the HOMO-1, HOMO, and LUMO have a proper nodal plan and the absorption band centered around 300 nm is assigned to a localized $\pi \rightarrow \pi^*$ transition, whereas the absorption band in the 400−600 nm region corresponds to the ICT between the TPA donor and the cyanoacetic acid acceptor end group. Therefore, $\lambda_{max}^{(1)}$ witnesses the electronic excitation that activates the energy-to-electricity conversion process of these DSSCs. Figure 1 also confirms the highly delocalized character of the frontier orbitals, which is typical of cyanine-like systems.

The experimental values of TPA dyes are measured in solution. Obviously, if we are to compare theoretical values with these data, the solvation effects have to be taken into account. Formally, and similarly to the BS impact, the solvent effects can also be split into direct and indirect components. The relative weight of both contributions is given in Table 3. According to the experimental setup, the selected solvents are methanol [MeOH, relative dielectric constant (EPS) of 32.63] and dichloromethane ($CH_2Cl_2$, EPS = 8.93). It turns out that the minor changes in the ground-state geometry due to solvation have no noticeable impact whatever the polarity of the solvent. In contrast, the excitation energies are strongly affected by the interactions with the solvent: the shift when going from vacuuo to dielectrico is close to + 30 (− 0.14 eV) and + 10 nm (−0.11 eV) for $\lambda_{max}^{(1)}$ and $\lambda_{max}^{(2)}$, respectively. While these shifts are very similar for both solvents, the incorporation of direct solvent effects is essential to maintain a satisfactory description of the auxochromic shifts.

The last computational parameter to fix is the functional(s) for the TDDFT calculations, and we compared the UV/vis performance of BHandH, O3LYP, B3LYP, and PBE0 hybrids with respect to the experimental measurements. We also tested the HF framework, to get a set of methods featuring a gradual decreasing fraction of exact exchange (from 50% for BHandH to 100% for HF).

**SCHEME 2: Sketch of the TPC, TC, and TPR Derivatives with the Numbering of the Substitution Positions**

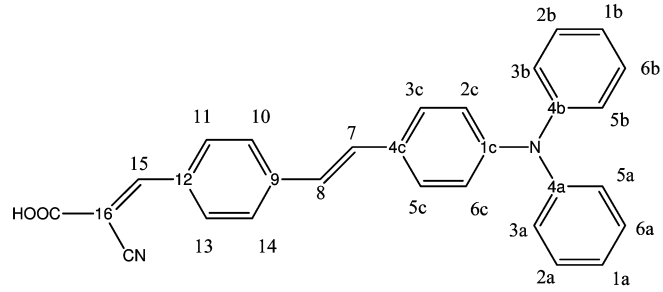


**TPC-1**

**TPC-2 : 11, 14-diBr**
**TPC-3 : 11, 14-diCl**
**TPC-5 : 11, 14-diCN**
**TPC-4 : 11,14-diThiophene**

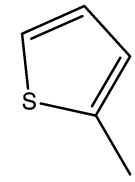


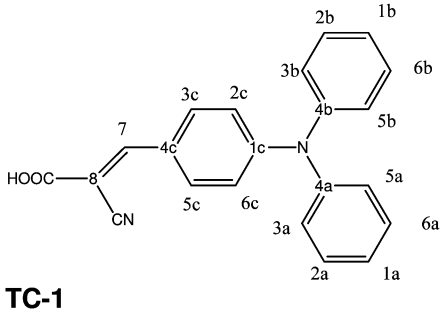


**TC-1**

**TC-2 : 1-Ethylene**
**TC-3 : 1-Cyanoacetic acid**

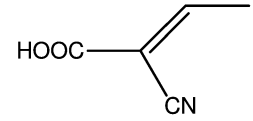


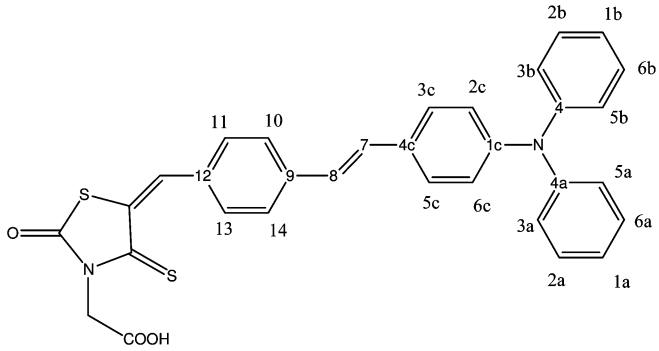


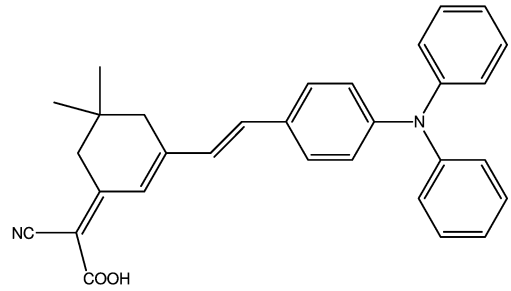


**TPR-1**
**TPR-2 : 11,14-diBr**

**TPR-3**

Since the crucial electronic excitation in this investigation is the ICT absorption band, and considering the fact that no experimental $\lambda_{max}^{(2)}$ values can be found in the literature for the class of TPA derivatives considered, we focus the methodological study on $\lambda_{max}^{(1)}$ only.

Table 4 presents a comparison between simulated and experimental $\lambda_{max}$. We consider a panel of 12 compounds indicative of TPA-m: TPC-1 to -6 (in TPC-6, the second phenyl bridging group, i.e., C9−C10−C11−C12−C13−C14, has been replaced by a furan group),[21] three TC derivatives, as well as three TPR compounds. For two of the TPRs, a rhodanine-3-acetic acid is the A group (see Scheme 2), and for TPR-3 the terminal group is a cyano-2-(5,5,-dimethylcyclohex-2-enyldiene) acetic acid.[18] Literature reports that TDDFT excitation energies are in general within a 0.4 eV deviation from experiment, and for organic dyes, the average errors are frequently smaller than this upper limit. For instance, Guillaumont and Nakamura calculated the maximum absorption wavelength of several organic dyes (indigo, azobenzene, phenylamine, hydrazone, and anthraquinone) with an average deviation close to 0.20 eV.[55] Also, Li et al. got the $\lambda_{max}$ of TPA methyl and carbonyl derivatives within a 0.63 eV deviation from experiment using the ZINDO/1-CI formalism.[56] Recently, Xu and co-workers studied the UV/vis spectrum of TC1 at the TDB3LYP/6-31G(d,p)//B3LYP/6-31G(d,p) level of theory, and they obtained an average error close to 0.64 eV for both $\lambda_{max}^{(1)}$ and $\lambda_{max}^{(2)}$.[20]

From the results listed in Table 4, it is obvious that BHandH is the functional of choice for the UV/vis spectra calculation. Indeed, on the basis of the agreement with experimental data by using the mean average error (MAE) and the mean signed error (MSE) criteria, the quality ranking of the hybrids for the $\lambda_{max}$ evaluation is BHandH (MAE, 18 nm/0.11 eV; MSE, 13

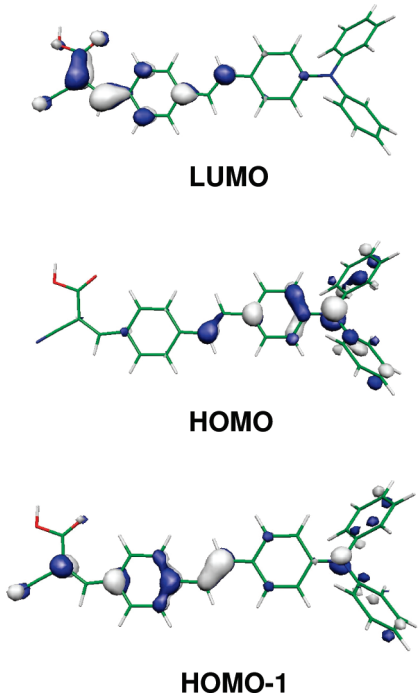


**Figure 1.** Representation of the TPA-m-COOH HOMO-1, HOMO, and LUMO. They have been obtained at the TDB3LYP/6-31G(d,p)// B3LYP/6-31G(d,p) level. For the TPA-m derivated dyes, the first excitation process involves a ICT HOMO → LUMO transition whereas the second excitation corresponds to a HOMO-1 → LUMO transition.

**TABLE 3: Solvent Effects on the Estimated $\lambda_{max}$ (in nm)[a]**

| geometry | gas | | | $CH_2Cl_2$ | | MeOH | |
|---|---|---|---|---|---|---|---|
| UV | gas | $CH_2Cl_2$ | MeOH | gas | $CH_2Cl_2$ | gas | MeOH |
| $\lambda_{max}^{(1)}$ | 478 | 504 | 505 | 478 | 505 | 479 | 507 |
| $\lambda_{max}^{(2)}$ | 350 | 360 | 361 | 350 | 360 | 351 | 362 |

[a] All values have been obtained at the TDB3LYP/6-31G(d,p)// B3LYP/6-31G(d,p) level of theory. The solvent effects are taken into account by the PCM approach.

nm/−0.07 eV), HF (MSE, 77 nm/0.58 eV), PBE0 (MSE, 125 nm/−0.58 eV), B3LYP (MSE, 162 nm/−0.71 eV), and O3LYP (MSE, 227 nm/−0.89 eV). As these results suggest, the percentage of the HF (exact) exchange is crucial and the estimated $\lambda_{max}$ decreases when increasing the amount of HF exchange incorporated in the functional.

In a recent work dealing with the relationship between spurious (charge transfer) excited states and the amount of exact exchange, Tretiak and Magyar[57] have examined the performance of various TDDFT functionals. Their study includes several polar donor−acceptor systems (including the (*E*)-4-(4-(methylsufonyl)styryl)-*N*,*N*-diphenylbenzenamine, a TPA derivative very similar to TPC-1) and molecular aggregates. For all the considered systems, the authors have demonstrated that a good description of the CT states can be achieved when a large fraction of HF exchange is used. Whilst the optimal fraction of exchange remains unknown, it appears that using a fraction ≥0.50 would result in a qualitatively correct physical description, but at the price of a possible overestimation of both the excitation energies and the oscillator strenghts.[58] These previous conclusions are indeed fully consistent with our results.

Note that the BHandH deviation is totally acceptable and in the line of a recently published PCM-TDDFT study on a large family of triphenylmethane very similar to TPA.[59,60] Note that our model provides deviations that are 2 orders of magnitude smaller than in the Guillaumont and Nakamura work,[55] and compared to the Li and co-worker ZINDO/1-CI results, the MAE is reduced by a factor 5.[56]

Regarding $\lambda_{max}^{(1)}$, the compounds listed in Table 4 can be classified into two phenomenological groups: (i) the TPR and TPC derivatives, for which the $\lambda_{max}^{(1)}$ absolute errors are in the 0.10−0.30 eV window, (ii) the TC derivatives with a TDDFT accuracy of 0.01−0.05 eV, once more highlighting that for TC compounds the CT is less important than for the TPC derivatives. This conclusion is nicely illustrated by the topology of the frontier molecular orbitals depicted in Figure 2 for both TPC1 and TC1.

Eventually, we can review the possible origins of the major discrepancies between theory and experiment: (i) the functionals used in this approach might not be optimal for describing the long-range effects though we are facing delocalized chromophores, but appropriate functionals are still not yet available in commercial QM packages; (ii) PCM does not explicitly consider solute−solvent specific interactions. However, dealing with specific interactions would require considering (at least), the molecules of the first solvation shell; (iii) the vibronic effects are not taken into account; (iv) the CT transition (for which one notices an important change of the dipolar moment between the ground and excited state) in solution could be more accurately described by using the state-specific PCM in which the cavity is reoptimized for each excited state.[61] While all these corrections are technically feasible for small systems, it would here require huge amounts of CPU ressources and would consequently ruin our approach, which we want to be as simple, fast, and as general as possible.

## Results

**Electron Injection.** In this section, we focus on the evaluation of the electrochemical properties of the dyes in their excited state. More precisely, we propose to establish a reliable theoretical scheme to quantify the electron injection onto a titanium dioxide ($TiO_2$) surface for selected TPA derivatives.

The free energy change (in eV) for the electron injection can be expressed as[62]

$$\Delta G^{\text{inject}} = E_{OX}^{dye*} - E_{CB}^{SC} \quad (1)$$

where $E_{OX}^{dye*}$ is the oxidation potential of the dye in the excited state, and $E_{CB}^{SC}$ is the reduction potential of the conduction band of the semiconductor. It is often difficult to accurately determine $E_{CB}^{SC}$ experimentally because it is sensitive to the surface conditions, as well as to the pH of the solution. Nevertheless, the $E_{CB}^{SC}$ values of several materials have been reported, and we have been using $E_{CB}^{SC} = 4.0$ eV for $TiO_2$.[63] The presented value has been experimentally determined and refers to conditions where the semiconductor is in contact with aqueous redox electrolytes of fixed pH.[64]

Two models can be used for the evaluation of $E_{OX}^{dye*}$. The first implies that the electron injection occurs from the unrelaxed excited state. For this reaction path, the excited-state oxidation potential can be extracted from the redox potential of the ground-state $E_{OX}^{dye}$, and the absorption energy associated to the photo-induced ICT ($\lambda_{max}^{(1)}$) according to[62]

$$E_{OX}^{dye*} = E_{OX}^{dye} - \lambda_{max}^{(1)} \quad (2)$$

**TABLE 4: $\lambda_{max}^{(1)}$ (in nm) Provided by PCM-TDO3LYP, PCM-TDB3LYP, PCM-TDPBE0, PCM-TDBHandH, and PCM-TDHF//6-311+G(2d,2p)[a]**

| | $\lambda_{max}^{(1)}$ | | | | | | | |
|---|---|---|---|---|---|---|---|---|
| compounds | O3LYP | B3LYP | PBE0 | BHandH | HF | exptl | solvent | ref |
| TPC-1 | 680 | 609 | 570 | 455 | 375 | 438 | $CH_2Cl_2$ | 19 |
| TPC-2 | 745 | 668 | 624 | 485 | 383 | 442 | $CH_2Cl_2$ | 19 |
| TPC-3 | 744 | 666 | 622 | 484 | 383 | 442 | $CH_2Cl_2$ | 19 |
| TPC-4 | 716 | 631 | 585 | 454 | 365 | 425 | $CH_2Cl_2$ | 19 |
| TPC-5 | 807 | 731 | 686 | 534 | 411 | 500 | $CH_2Cl_2$ | 19 |
| TPC-6 | 645 | 594 | 562 | 478 | 415 | 469 | THF | 21 |
| TC-1 | 489 | 465 | 448 | 392 | 315 | 400 | MeOH | 20 |
| TC-2 | 516 | 486 | 466 | 402 | 331 | 403 | MeOH | 20 |
| TC-3 | 541 | 511 | 488 | 418 | 329 | 416 | MeOH | 20 |
| TPR-1 | 767 | 666 | 615 | 473 | 381 | 468 | $CH_2Cl_2$ | 19 |
| TPR-2 | 818 | 706 | 650 | 485 | 380 | 480 | $CH_2Cl_2$ | 19 |
| TPR-3 | 622 | 578 | 550 | 462 | 383 | 487 | $CHCl_3$ | 18 |
| MAE | 227 (0.89) | 162 (0.71) | 125 (0.58) | 18(0.11) | 77(0.58) | | | |
| MSE | 227 (−0.89) | 162 (−0.71) | 125 (−0.58) | 13(−0.07) | −77(0.58) | | | |

[a] All geometries are obtained at the B3LYP/6-31G(d,p) level. We also provide the MAE and MSE in nm (in eV).

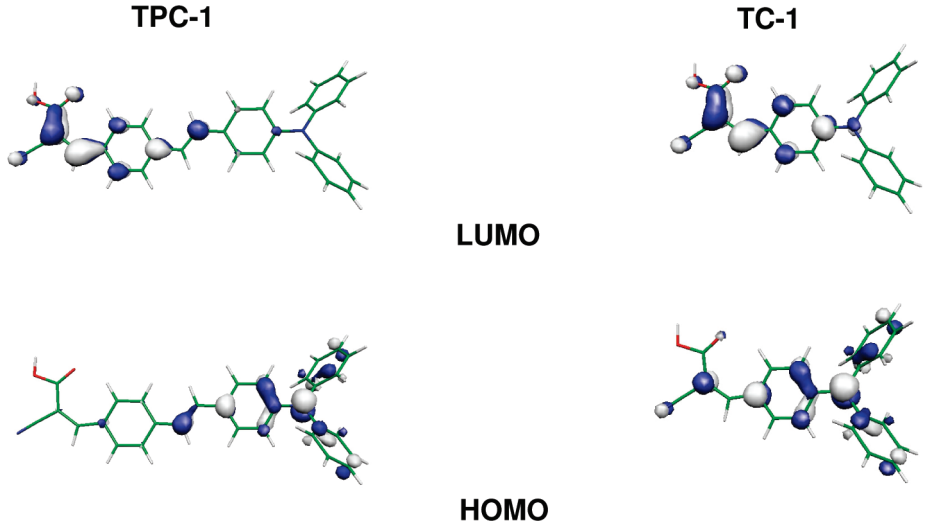


**Figure 2.** Comparison between the TPC-1 and TC-1 HOMO and LUMO associated to the $\lambda_{max}^{(1)}$ transition. They have been obtained at the TDB3LYP/6-31G(d,p)//B3LYP/6-31G(d,p) level.

Note that this relation is only valid if the entropy change during the light absorption can be neglected. For the second model, we assume that electron injection occurs after relaxation. Given this condition, $E_{OX}^{dye^*}$ is expressed as[62]

$$E_{OX}^{dye^*} = E_{OX}^{dye} - E_{0-0}^{dye} \quad (3)$$

where $E_{0-0}^{dye}$ is the energy difference between the ground state and the relaxed excited state.

To calculate the 0−0 "absorption" line, we need both the $S_0$ (singlet ground state) and the $S_1$ (first singlet excited state) equilibrium geometries. More precisely, the 0−0 transition energy is calculated as

$$E_{0-0} = \lambda_{max}^{(1)} - E_{S_1}^{reorg} \quad (4)$$

where

$$E_{S_1}^{reorg} = E_{S_1}(\mathbf{Q}_{S_0}) - E_{S_1}(\mathbf{Q}_{S_1}) \quad (5)$$

and

$$E_{S_1}(\mathbf{Q}_{S_0}) = E_{S_0}(\mathbf{Q}_{S_0}) + \Delta E_{S_1} \quad (6)$$

$\mathbf{Q}_{S_0}$ and $\mathbf{Q}_{S_1}$ are the equilibrium geometries for the $S_0$ and $S_1$ states, respectively. $E_{S_1}(\mathbf{Q}_{S_0})$ and $E_{S_1}(\mathbf{Q}_{S_1})$ denote the internal energies for the $S_1$ state calculated at $\mathbf{Q}_{S_0}$ and $\mathbf{Q}_{S_1}$, respectively, whereas $\Delta E_{S_1}$ is the $S_0 \rightarrow S_1$ excitation energy. Up to now, geometry optimization in the solvent phase of the excited singlet states at the TDDFT level is not available in standard QM packages. However, in a recent work, Cave, Burke, and Castner calculated the fluorescence spectra of coumarin derivatives at the DFT level and propose to use the geometry of the $T_1$ state as an estimate of the $S_1$ equilibrium geometry.[65,66] Indeed, since both the $S_1$ and $T_1$ states are strongly characterized by a HOMO → LUMO contribution, it is tenable to postulate that their equilibrium geometries are quite similar. In this work, the geometry optimization for the $S_1$ [$T_1$] state is performed at the [U]B3LYP/6-31G(d,p) level, and for the sake of consistency, $\Delta E_{S_1}$ has been calculated using the same functional with the 6-311G+(2d,2p) BS. The parameters used in eqs 5 and 6 for the evaluation of $E_{S_1}^{reorg}$ of TPC-1

**TABLE 5: Estimated $E_{0-0}$ and $E^{reorg}_{S_1}$ for TPC-1 and TPC-2 (in eV)[a]**

| scheme | $\Delta E_{S_1}$ | $E^{reorg}_{S_1}$ | $\lambda^{(1)}_{max}$ | $E_{0-0}$ |
|---|---|---|---|---|
| | | TPC-1 | | |
| gas | 2.24 | 0.59 | 2.90 | 2.31 |
| $CH_2Cl_2$ | 2.03 | 0.51 | 2.73 | 2.22 |
| | | TPC-2 | | |
| gas | 2.09 | 0.49 | 2.76 | 2.07 |
| $CH_2Cl_2$ | 1.86 | 0.46 | 2.56 | 2.10 |

[a] The PCM has been used to take into account the solvent effects.

**TABLE 6: Estimated $\Delta G^{inject.}$, $E^{dye}_{OX}$, and $E^{dye*}_{OX}$ (in eV) for TPC-1 and TPC-2 Following Both the Relaxed and Unrelaxed Paths of Reaction[a]**

| scheme | $\Delta G^{inject}$ | $E^{dye}_{OX}$ | $E^{dye*}_{OX}$ | $E^{dye}_{OX\text{-}Exp}$ | ref |
|---|---|---|---|---|---|
| | | TPC-1 | | | |
| | | gas | | | |
| relaxed | −0.13 | 6.18 | 3.87 | | |
| unrelaxed | −0.72 | 6.18 | 3.28 | | |
| | | $CH_2Cl_2$ | | | |
| relaxed | −1.33 | 4.89 | 2.67 | | |
| unrelaxed | −1.84 | 4.89 | 2.16 | 5.47 | 19 |
| | | TPC-2 | | | |
| | | gas | | | |
| relaxed | 0.27 | 6.34 | 4.27 | | |
| unrelaxed | −0.42 | 6.34 | 3.58 | | |
| | | $CH_2Cl_2$ | | | |
| relaxed | −1.11 | 4.99 | 2.89 | | |
| unrelaxed | −1.57 | 4.99 | 2.43 | 5.54 | 19 |

[a] We also compare the theoretical $E^{dye}_{OX}$ to the experimental value (in eV). For both reaction paths, we have considered the electron injection in gas and solvent phase. These parameters are obtained using the restricted and unrestricted B3LYP functional combined with the 6-31G(d,p) basis set. The PCM has been use to take into account the solvent effects.

and TPC-2 in both gas and solvent phase are given in Table 5. It turns out that the difference between gas and solvent phase $E^{reorg}_{S_1}$ is strongly compound-dependent, slightly influenced by the solvent effects and remains quite modest in total, i.e., $E^{reorg}_{S_1}$ only amounts to 10% of the ICT excitation energy. Note that the zero-point correction (ZPC) in the $E^{reorg}_{S_1}$ gas phase calculations is weak ($E^{reorg}_{S_1-ZPC}$ amounts to 0.66 and 0.55 eV, for TPC-1 and TPC-2, respectively) and can therefore be neglected.

In Table 6, we provide the $\Delta G^{inject}$, as well as $E^{dye}_{OX}$ and $E^{dye*}_{OX}$ (in eV) for two representative dyes, TPC-1 and TPC-2, following both the relaxed and unrelaxed reaction paths in gas and solvent phase. From these results, one can conclude that (i) for both paths, the effect of the dielectric surroundings on $\Delta G^{inject}$ value is huge, with a shift of ∼−1.0 eV when going from gas to dichloromethane. Note that the shift of the $E^{dye}_{OX}$ is almost similar for TPC-1 and TPC-2 and amounts to ∼ −1.3 eV. As expected, the main solvent effect results in a stabilization of the oxidized dye and favors the electron injection; (ii) the $\Delta G^{inject}_{relaxed} > \Delta G^{inject}_{unrelaxed}$, that is the injection driving force is more important when an electron is ejected from a higher energetic valence excited state;[67,68] (iii) the anodic displacements of $E^{dye}_{OX}$ and $E^{dye*}_{OX}$ are in good agreement with experimental data. For instance, when going from TPC-1 to TPC-2, one calculates an anodic shift of 0.10 and 0.27 eV for $E^{dye}_{OX}$ and $E^{dye*}_{OX}$ (using the unrelaxed scheme), whereas the experimental displacements are 0.04 ± 0.01 and 0.11 ± 0.01 eV, respectively; (iv) while the $E^{dye}_{OX}$ displacements ($\Delta E^{dye}_{OX}$) are quantitatively well reproduced, the absolute $E^{dye}_{OX}$ values suffer a limited accuracy of ±0.45 eV.

**TABLE 7: Estimated $\Delta G^{inject}$, $E^{dye}_{OX}$, and $E^{dye*}_{OX}$ (in eV) for TPC-3 and TPC-5, As Well As for TC-1, TC-2, and TC-3 Following the Unrelaxed Path of Reaction[a]**

| scheme | $\Delta G^{inject}$ | $E^{dye}_{OX}$ | $E^{dye*}_{OX}$ | $E^{dye}_{OX\text{-}Exp}$ | ref |
|---|---|---|---|---|---|
| TPC-3 | gas | | | | |
| | −0.49 | 6.28 | 3.51 | | |
| | $CH_2Cl_2$ | | | | |
| | −1.60 | 4.96 | 2.40 | 5.56 | 19 |
| TPC-5 | gas | | | | |
| | −0.08 | 6.46 | 3.92 | | |
| | $CH_2Cl_2$ | | | | |
| | −1.32 | 5.00 | 2.68 | 5.57 | 19 |
| TC-1 | gas | | | | |
| | −0.69 | 6.67 | 3.31 | | |
| | $CH_3CN$ | | | | |
| | −2.05 | 5.11 | 1.95 | 5.44 | 20 |
| TC-2 | gas | | | | |
| | −0.76 | 6.52 | 3.24 | | |
| | $CH_3CN$ | | | | |
| | −2.06 | 5.02 | 1.94 | 5.48 | 20 |
| TC-3 | gas | | | | |
| | −0.25 | 6.89 | 3.75 | | |
| | $CH_3$ CN | | | | |
| | −1.67 | 5.30 | 2.33 | 5.56 | 20 |

[a] For both reaction paths, we have considered the electron injection in gas and solvent phase. For the set of five compounds, we compare the theoretical $E^{dye}_{OX}$ to the experimental value (in eV). The theoretical parameters presented here are obtained using the restricted and unrestricted B3LYP functional combined with the 6-31G(d,p) basis set. The PCM has been used to take into account the solvent effects.

However, since $\Delta E^{dye}_{OX}$ remains the truly crucial parameter, our procedure can be used to predict new optimal structures for DSSc applications.

Though electron injection from unrelaxed excited states has been observed in $TiO_2$[69] and $SnO_2$,[70,71] the relative contribution of an ultrafast injection path is not clear, and the experimentators commonly assume that electron injection dominantly occurs after relaxation.[62] However, the results displayed in Table 6 reveal that the absolute difference between the relaxed and unrelaxed $\Delta G^{inject}$ is constant and amounts to ∼0.5 eV, which is of the same order of magnitude than the $E^{dye}_{OX}$ and $E^{dye*}_{OX}$ MAE (±0.45 eV). Consistently, in order to keep the fast and simple character of our methodology, we strive for the unrelaxed path of injection for the $\Delta G^{inject}$ evaluation of new dyes.

In order to confirm the reliability of the procedure for the evaluation of the $\Delta G^{inject}_{unrelaxed}$, we have performed a blind test on a set of the five additional systems listed in Table 7, in which we also confront our theoretical $E^{dye}_{OX}$ to experimental data. A comparison between gas and solvent phase oxidation potentials allows to conclude that the $E^{dye}_{OX}$ cathodic shift induced by the solvent is only loosely sensitive to the permittivity of the surroundings. Indeed, the TPC-series shift is −1.35 eV in $CH_2Cl_2$, while the average $\Delta E^{dye}_{OX}$ in $CH_3CN$ amounts −1.60 eV. Second, in the series TPC-1 → TPC-2 → TPC-3 → TPC-5, experiments show a slight anodic shift (∼0.10 eV between TPC-1 and TPC-5) that is perfectly reproduced by the theory, going from 4.89 to 5.00 eV (TPC-5) in solution. For the TC series, the anodic shift observed when a second cyanoacetic derivated acid is grafted on TC-1 is also well reproduced by the theory, as the experimental value of 0.19 eV compares to our calculated 0.12 eV. On the contrary, our methodology is unable to reproduce the experimental $E^{dye}_{OX}$ order for this series (TC-1 < TC-2 < TC-3), the oxidation potential of TC-2 being underestimated. Aside the usual origins of discrepancies between theory and experiment, such as the well-known PCM

**TABLE 8: Estimated (Relative) $\Delta G^{inject}$ ($\Delta G_r^{inject}$), $E_{OX}^{dye}$, and $E_{OX}^{dye*}$ (in eV) for a Series of New Structures (See Scheme *3*) Following the Unrelaxed Path of Reaction[a]**

| Compounds | | $\Delta G^{inject.}$ | $E_{OX}^{dye}$ | $E_{OX}^{dye*}$ | $\lambda_{max}^{(1)}$ | $f$ | RLHE | $\Delta G_r^{inject.}$ |
|---|---|---|---|---|---|---|---|---|
| | TPC-1 | −1.84 | 4.89 | 2.16 | 2.73 | 1.8976 | 0.9000 | 1.00 |
| 11,14-diBr-TPC-1 | TPC-2 | −1.57 | 4.99 | 2.43 | 2.56 | 1.7565 | 0.8813 | 0.85 |
| 11,14-diCl-TPC-1 | TPC-3 | −1.60 | 4.96 | 2.40 | 2.56 | 1.7857 | 0.8854 | 0.87 |
| 11,14-diCN-TPC-1 | TPC-5 | −1.32 | 5.00 | 2.68 | 2.32 | 1.6438 | 0.8640 | 0.72 |
| | TPC-6 | −1.73 | 4.86 | 2.27 | 2.59 | 2.0667 | 0.9186 | 0.94 |
| | TPR-1 | −1.85 | 4.77 | 2.15 | 2.62 | 1.9853 | 0.9101 | 1.01 |
| 1a,1b-diCl-TPC-1 | TPC-7 | −1.77 | 5.02 | 2.23 | 2.79 | 1.9721 | 0.9086 | 0.96 |
| 1a,1b-diF-TPC-1 | TPC-8 | −1.83 | 4.92 | 2.17 | 2.75 | 1.9365 | 0.9046 | 0.99 |
| 15-CN-TPC-1 | TPC-9 | −1.37 | 4.90 | 2.63 | 2.27 | 1.2993 | 0.7933 | 0.74 |
| 11,14-diF-TPC-1 | TPC-10 | −1.69 | 4.91 | 2.31 | 2.60 | 1.8551 | 0.8947 | 0.92 |
| 1a,1b-diOMe-11,14-diCl-TPC-1 | TPC-11 | −1.42 | 5.03 | 2.58 | 2.45 | 1.7505 | 0.8805 | 0.77 |
| 7,8-diCl-TPC-1 | TPC-12 | −2.75 | 5.11 | 1.25 | 3.86 | 1.2766 | 0.7876 | 1.49 |
| | TPC-13 | −1.99 | 5.03 | 2.01 | 3.02 | 1.2945 | 0.7921 | 1.08 |
| | TPC-14 | −1.93 | 4.65 | 2.07 | 2.58 | 2.3510 | 0.9423 | 1.05 |
| | TPC-15 | −2.79 | 3.66 | 1.21 | 2.45 | 2.7977 | 0.9665 | 1.52 |
| | TPC-16 | −1.85 | 4.97 | 2.15 | 2.82 | 1.8385 | 0.8926 | 1.01 |
| | TPC-17 | −1.94 | 4.78 | 2.06 | 2.72 | 1.9037 | 0.9007 | 1.05 |
| | TPC-18 | −2.20 | 5.16 | 1.80 | 3.36 | 1.7432 | 0.8794 | 1.20 |
| | TPC-19 | −2.39 | 4.94 | 1.61 | 3.33 | 1.8163 | 0.8896 | 1.30 |
| | TPC-20 | −1.99 | 5.25 | 2.01 | 3.24 | 1.5461 | 0.8468 | 1.08 |
| | TPC-21 | −1.66 | 4.87 | 2.34 | 2.53 | 2.0342 | 0.9153 | 0.90 |

[a] For each compound, we also provide the $\lambda_{max}^{(1)}$ (in eV), the corresponding oscillator strength ($f$), and the relative light-harvesting efficiency (RLHE). The theoretical parameters presented here are obtained using the restricted and unrestricted B3LYP functional combined with the 6-31G(d,p) basis set. The solvent is dichloromethane, and therefore, we correct the gas phase oxidation potential by 1.35 eV (see the Electron Injection section for more details). The $\lambda_{max}^{(1)}$'s (in eV) are obtained using the PCM model at the TDBHandH/6-311+G(2d,2p) level. The electrochemical parameters obtained for the new structures are also compared to the TPC-1, TPC-2, TPC-3, TPC-5, and TPC-6, as well as TPR-1 properties.

or DFT methods limitations (see the Setting up the Procedure section for more details), another source of error exists for TPC-2, that is, the free rotation around the bond between the ethylene unit and the phenyl might be activated and the lack of such twisted geometries in our model could explain the difficulty to correctly describe the electrochemical properties of these derivatives.

**Effects of Chemical Modifications.** In the present section, we propose structural modifications improving the electron injection efficiency of the TPA-based DSSCs. Of course, all modifications are theoretically possible and a large panel of new structures can be tested. Therefore, we impose that all dyes possess a least a terminal −COOH group on the acceptor unit, as the carboxylic group is necessary to link the dye to the semiconductor surface.[18] We focus on three properties that can be optimized—(i) the free energy of injection $\Delta G^{inject}$ in $TiO_2$ has to be less than −1.84 eV, the referential value calculated for TPC-1. Indeed, the larger $\Delta G^{inject}$, the faster the electron injection from the valence excited state. This assumption is valid as long as the injection is restricted to energy levels close to the conduction band edge and that the density of the acceptor states in this energy range remains constant;[68] (ii) the oxidation potential of the dyes must be more positive than the $I^-/I_3^-$ redox couple (4.8 ± 0.1 eV),[72] ensuring that there is enough driving force for a fast and efficient regeneration of the dye cation radical; and (iii) the light harvesting efficiency (LHE) of the dye has to be as high as possible to maximize the photocurrent response. More precisely, LHE is expressed as[73]

$$\mathrm{LHE} = 1 - 10^{-A} = 1 - 10^{-f} \qquad (7)$$

where $A$ ($f$) is the absorption (oscillator strength) of the dye associated to the $\lambda_{max}^{(1)}$. It is known that TDDFT is less efficient for the evaluation of transition probabilities than for transition energies. For the sake of computational consistency, the LHE criterion has therefore to be underweighted in our classification, as our estimates of $\Delta G^{inject}$ and $E_{OX}^{dye}$ are probably more reliable. However, we have to underline that the dependence of the experimental extinction coefficient with respect to auxochromic effects was qualitatively reproduced for the triphenylmethane derivatives.[59]

These three criteria have been followed to set up an efficiency ranking of the compounds listed in Table 8. In this table, we provide the $\Delta G^{inject}$, as well as the ground and excited state oxidation potentials for the set of 20 species displayed in Schemes 2 and 3. According to the conclusions drawn from the evaluation of $\Delta G^{inject}$ (see the Electron Injection section), we have considered that the electron injection occurs from the unrelaxed excited state of the dye. Additionally, as it has been shown that $CH_2Cl_2$ induces a −1.35 eV cathodic shift of $E_{OX}^{dye}$ for all compounds and that the dielectric constant of the medium leaves this shift almost unchanged, the solvent phase oxidation potential can simply be evaluated as $E_{OX\text{-}solvent}^{dye} = E_{OX\text{-}gas}^{dye} - 1.35$ eV.

Before starting our ranking, it has been checked that all the compounds listed in Table 8 show a higher oxidation potential than the $I^-/I_3^-$ redox potential (±4.8 eV). In this context, even though TPC-15 has both the highest LHE (2.7977) and injection driving force ($\Delta G^{inject} = -2.79$ eV), it must be discarded because its oxidation potential is 3.66 ± 0.45 eV. Moreover, in the TPC-15 peculiar case, the rodlike part is extended and it may facilitate the recombination of electrons to the electrolyte and favor the $\pi-\pi$ aggregation between molecules. Moreover, this $\pi-\pi$ aggregation can not only lead to both self-quenching of electron injection into $TiO_2$ but also to the instability of the organic dye due to the formation of excited triplet states or unstable radicals under light irradiation.[15,74,75] Note that we do decide not to exclude TPC-14, TPC-17, nor TPR-1, though their $E_{OX}^{dye}$ are quite close to the $I^-/I_3^-$ redox potential (4.65 eV, 4.78, and 4.77 eV,

**SCHEME 3: Sketch of the TPC-13−TPC-20 Derivatives**

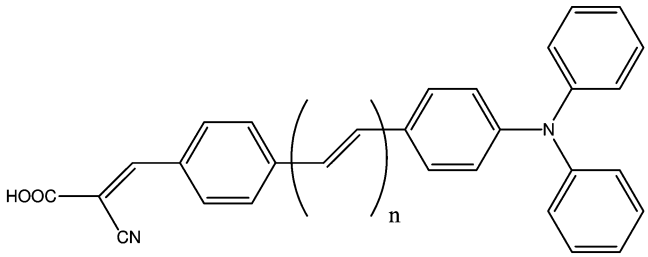


**TPC-13 : n = 0**
**TPC-1 : n = 1**
**TPC-14 : n = 2**
**TPC-15 : n = 3**

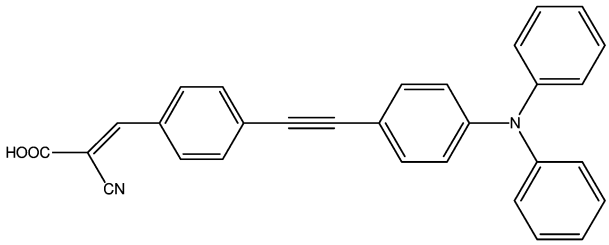


**TPC-16**

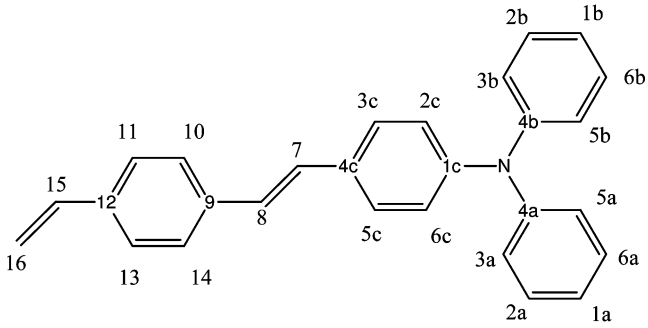


**TPC-17 : 16-diCOOH**
**TPC-18 : 16-COOH, 15-OMe, 1a,6b-diCN**
**TPC-19 : 16-OH, 16-COOH, 11,13-diOMe, 1a,6b-diCN**
**TPC-20 : 16-COOH, 15-CN, 11,13-diOMe, 1a,6b-diCN**

respectively), i.e., the difference between $E_{OX}^{dye}$ and the $I^-/I_3^-$ redox potential is lower than the precision (±0.45 eV) of our predictions.

With respect to the relative free energies of injection ($\Delta G_r^{inject} = \Delta G_{dye}^{inject}/\Delta G_{TPC\text{-}1}^{inject}$) and the relative LHE (RLHE, which is also obtained using eq 7 with the ratio $f^{dye}/f^{TPC\text{-}1}$ instead of $f$), the compounds listed in Table 8 obey five rules: (i) TPC-6, TPC-7, TPC-8, TPC-14, TPC-17, and TPR-1 derivatives show a LHE superior to TPC-1; (ii) the TPC-12, TPC-18, and TPC-19 have $\Delta G^{inject} < -2.00$ eV; (iii) TPC-17, TPC-14, and TPR-1 show only a slight improvement of both RLHE and $\Delta G^{inject}$ with respect to TPC-1; (iv) for the set of the test compounds listed in Table 8, apart from TPC-15 (that we have already discarded), it is impossible to isolate one valuable structure that shows a huge improvement of both the LHE and the injection driving force; (v) the −CN group grafted on the TPC-1-core in position 15 (TPC-9) or in positions 11 and 14 (TPC-5) significantly deteriorates the RLHE and the free energy of injection.

For the series TPC-13−TPC-15, the results reveal that the RLHE factor increases with the bridge length in the order TPC-13 (0.7921) < TPC-1 (0.9000) < TPC-14 (0.9423) < TPC-15 (0.9665). On the other hand, by adding (TPC-14) or removing (TPC-13) an ethylene group between the two phenyls of TPC-1, one does not significantly modify the $\Delta G_r^{inject}$ value, that is, only the oscillator strength is strongly affected. For TPC-13, this modification of $f$ is likely related to the loss of coplanarity between the two phenyls (a 30° out-of-plane distortion) and the conjugation of the acceptor−donor system is altered, which explains the smaller oscillator strength. Note that the reduction of the ethylene bridge in TPC-1 (which gives TPC-16) does not bring any improvement of the dye properties. For the TPC-6 and TPC-21 derivatives, we only notice a slight change in the RLHE (+0.02 in average) but a deterioration of the $\Delta G_r^{inject}$ factor which is explained by the important decrease (∼0.2 eV in average) of the excitation energies when the terminal phenyl group of TPC-1 has been replaced by a furan (TPC-6) or a thiophene (TPC-21) group.

From the whole original set of new potential structures listed in Table 8, only two types of dyes finally retain our attention: (i) TPC-18, TPC-19, and TPC-20 because of their $\Delta G_r^{inject} >$ 1.00 (1.20, 1.30 and 1.08, respectively) and LHE that are very close to TPC-1. For these dyes, the high $\Delta G_r^{inject}$ value can be explained by the huge variation of the $\lambda_{max}^{(1)}$ (when going from TPC-1 to TPC-19, $\Delta\lambda_{max}^{(1)} = 0.60$ eV), much larger than the $E_{OX}^{dye}$ variation (+0.05 eV). (ii) TPC-14, as this compound shows the highest RLHE index with a $\Delta G_r^{inject}$ superior to TPC-1.

**Molecular Orbital Analysis.** To get further insights into the molecular structure and electronic distribution of these organic dyes, we have performed a molecular orbital analysis (MOA) at the B3LYP/6-31G(d,p) level of theory. The electron distributions for the HOMO and LUMO of TPC-1, TPC-12, TPC-14, TPC-18, TPC-19, and TPC-20 are depicted in Figures 3 and 4. For all the considered systems but TPC-19, the HOMO is essentially localized on the central nitrogen atom whereas the LUMO is located in anchoring group through the $\pi$-bridge. For the TPC derivatives but TPC-20, the MOA reveals that the cyanoacrylic acid group is essentially coplanar to the phenyl acceptor group. It is also important to underline that, in view of the frontier orbitals topology of TPC-1, TPC-12, TPC-14, TPC-18, and TPC-20, the HOMO → LUMO excitation induced by light irradiation could move the electron distribution from the TPA moiety to the anchoring group. Therefore, assuming a similar molecular orbital shape when the dye is anchored to $TiO_2$, the LUMO centered on the anchoring moiety should enhance the orbital overlap with the titanium 3d orbital and subsequently favor the electron injection to the $TiO_2$ matrix. Note that by grafting several EDGs (electron donating groups) on the dye tail, one induces a strong modification of the HOMO and LUMO electronic distribution. This alteration of the electronic structure is much obvious for TPC-19, as for this compound, one observes that during the excitation, the charge transfer occurs from the acceptor to the bridge. By grafting several EDGs on the acceptor moiety, one reverses the direction of the induced ICT and the amount of negative charge at the $TiO_2$-dye interface dramatically decreases, which probably impedes an efficient injection. Furthermore, the LUMO of TPR-1 (see Figure 5) is mainly centered on the rhodanine, especially on the carbonyl and thiocarbonyl groups, leaving the LUMO isolated from the −COOH anchoring group. Consequently in TPR-1, electrons are far from being efficiently injected into the $TiO_2$ conducting band via the carboxyl group. This theoretical analysis is in complete agreement with the experimental observations.[76]

**Optimal Structures.** From the conclusions of the Effects of Chemical Modifications and Molecular Orbital Analysis sec-

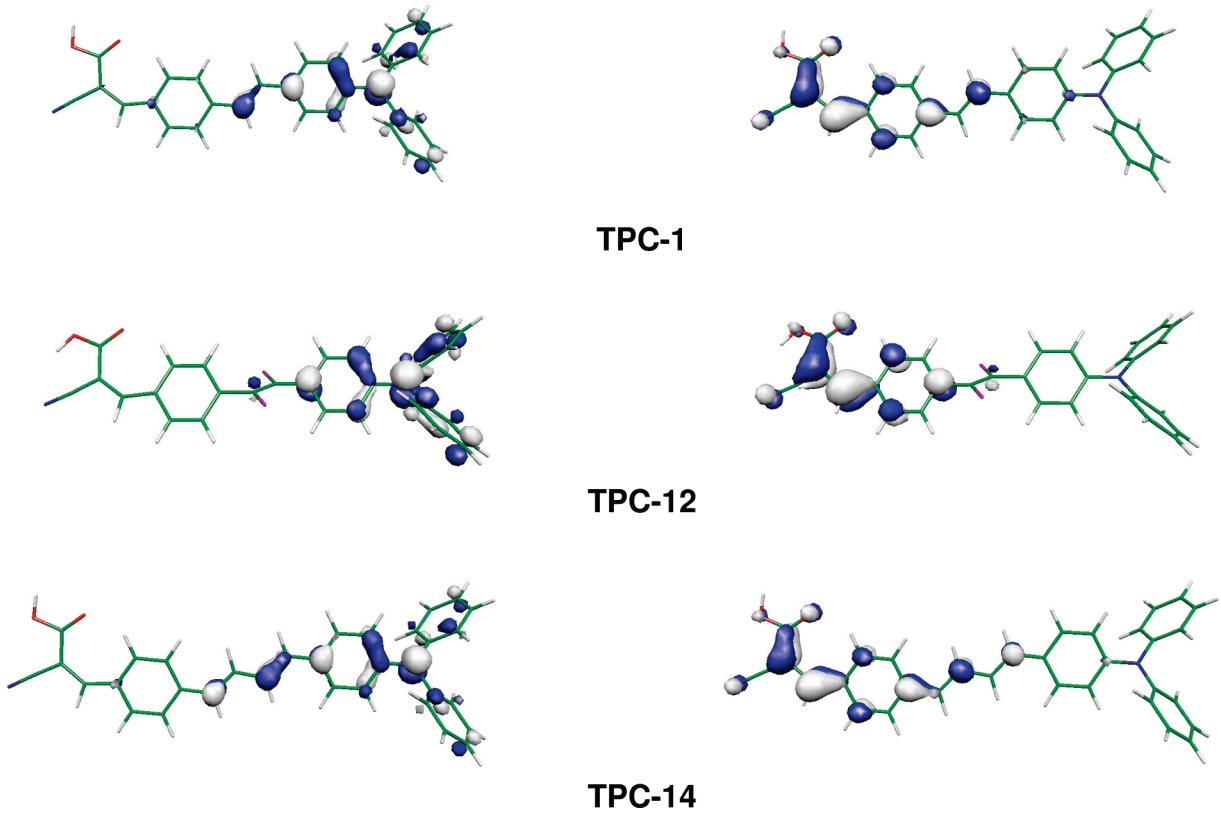


**Figure 3.** Comparison between the TPC-1, TPC-12, and TPC-14 HOMO (left) and LUMO (right) associated to the $\lambda_{max}^{(1)}$ transition. They have been obtained at the TDB3LYP/6-31G(d,p)//B3LYP/6-31G(d,p) level.

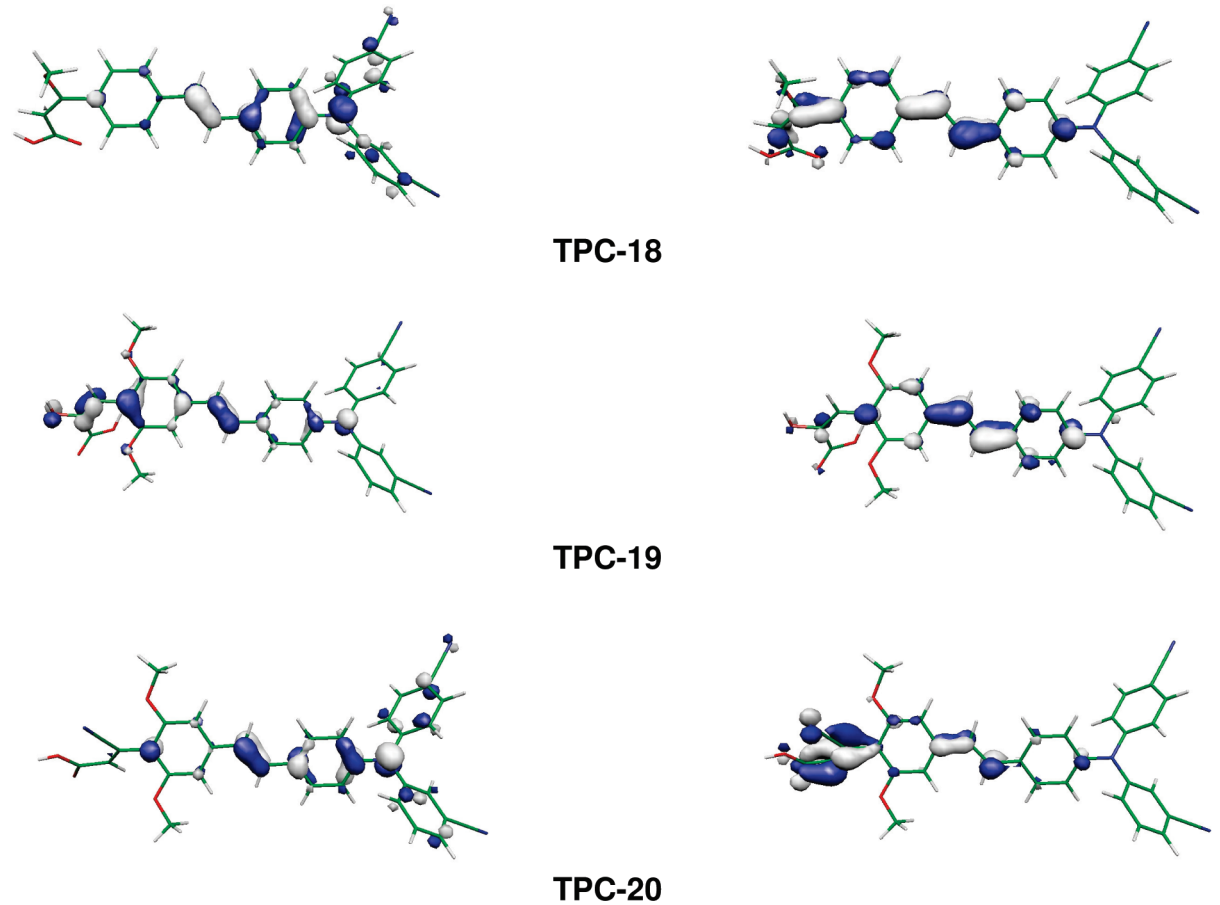


**Figure 4.** Comparison between the TPC-18, TPC-19, and TPC-20 HOMO (left) and LUMO (right) associated to the $\lambda_{max}^{(1)}$ transition. They have been obtained at the TDB3LYP/6-31G(d,p)//B3LYP/6-31G(d,p) level.

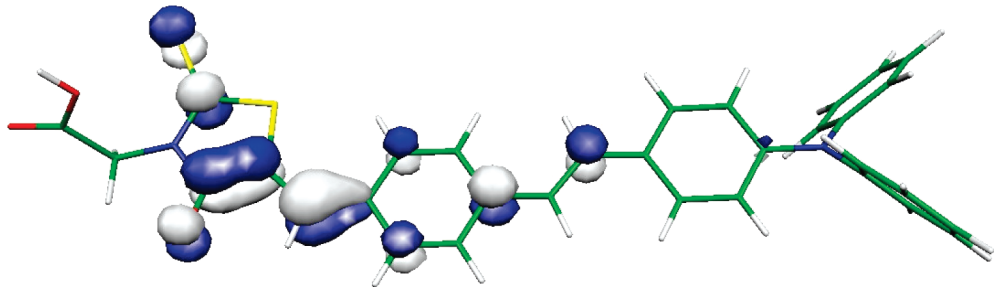

**Figure 5.** TPR-1 LUMO topology obtained at the TDB3LYP/6-31G(d,p)//B3LYP/6-31G(d,p) level.

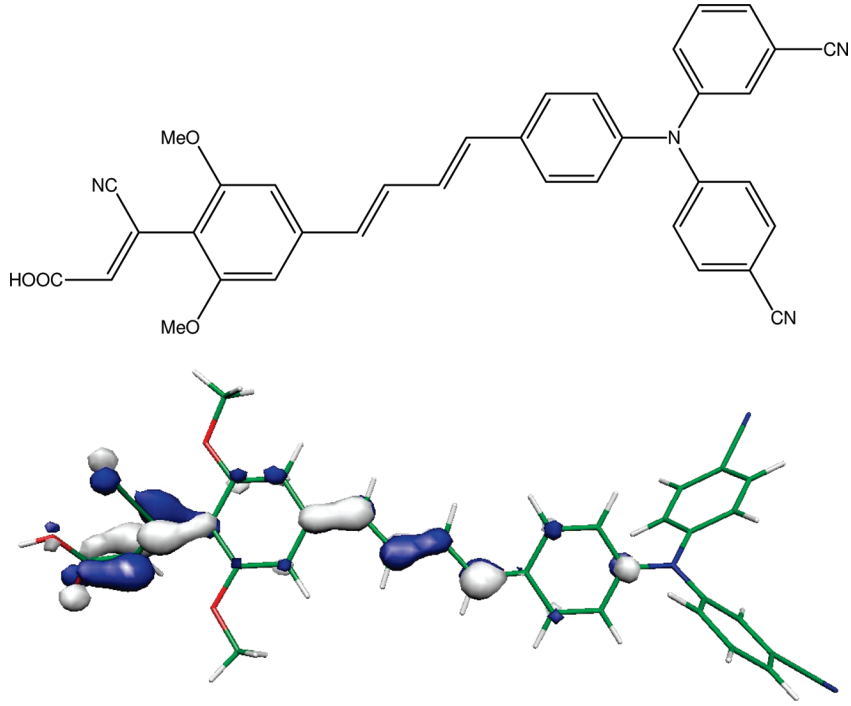


**Figure 6.** Sketch of the TPC-23 (up) derivatives and its LUMO (bottom) which has been obtained at the TDB3LYP/6-31G(d,p)//B3LYP/6-31G(d,p) level.

tions, we can propose two structures that are expected to show the "best" photovoltaic properties, at least as good as the three TPC-14, TPC-18, and TPC-20 dyes. More precisely, both the "optimal" structures (TPC-22 and TPC-23) contain two ethylene units between the two bridging phenyls, a −COOH group in position 16 and a 1a,6-diCN functionalization. TPC-22 is obtained by grafting a −OMe in position 15, whereas in TPC-23 the 15-OMe is replaced by a 15-CN group and two −OMe functions are added in positions 1 and 13. These two prototypes absorb at 2.68 ($f$ = 1.9492) and 3.05 eV ($f$ = 2.1210), respectively. These two new structures are characterized as follows. (i) The $E_{OX}^{dye}$ ($E_{OX}^{dye*}$) of TPC-22 and TPC-23 are 4.99 (2.31 eV) and 5.04 eV (1.99 eV), respectively; (ii) the $\Delta G^{inject}$ amount to −1.69 and −2.01 eV for TPC-22 and TPC-23, respectively. Going from TPC-1 to TPC-22 leads to a huge deterioration of the $\Delta G^{inject}$ which is explained by the increase of $E_{OX}^{dye*}$ (from 2.16 to 2.31 eV). Clearly, TPC-22 must be discarded because it does not provide the expected improvement of the electron injection.

For the series TPC-14, TPC-18, TPC-20, and TPC-23, we obtain the following RLHE order: TPC-14 (0.9423) > TPC-23 (09217) > TPC-18 (0.8794) and TPC-20 (0.8468). For $\Delta G^{inject}$ we get TPC-18 (−2.20 eV) > TPC-23 (−2.01 eV) > TPC-20 (−1.99 eV) > TPC-14 (−1.93 eV). For TPC-22, the fusion of TPC-20 and TPC-14 lead to a compound that show an intermediate RLHE value and a higher injection driving force.

Figure 6 shows that for TPC-23, the LUMO is centered on the anchoring moiety and would therefore favor the electron injection from dye to the semiconductor. Furthermore, the evaluation of the atomic charge carried by the nitrogen ($q^N$ in $|e|$) at the TPA level confirms the DSSC abilities of TPC-23. As underlined in the Introduction, the cationic TPA moiety locates the positive charge far away from the semiconductor surface after injection and efficiently restricts the recombination process. To evaluate $q$, we used the B3LYP/6-31G(d,p) gas-phase charges derived from the electrostatic potential (MK charges or Merz−Singh−Kollman scheme).[77] For TPC-1, the variation of the charge ($\Delta q^N$) between the neutral ($q_{dye}^N = -0.4695\ |e|$) and cationic species ($q_{dye^+}^N = -0.3409\ |e|$) amounts to 0.1286 $|e|$, whereas for TPC-23 the variation is negligible (0.0175 $|e|$) and the positive charge is completely diluted in the conjugated bridging group. Of course, several experimental factors have to be considered for the treatment of the recombination. However, for TPC-23, since the coplanarity between the −CHCN−CHCOOH anchoring group and its bridging unit is broken (∼60° out-of-plane distortion), one can assume that the positive charge may not be directly in contact with the $TiO_2$ surface and that the recombination reaction would therefore be partly inhibited.

## Concluding Remarks

In the present work, we managed (i) to establish a theoretical procedure able to evaluate the absorption spectra of TPA derivatives in several solvents, (ii) to use this theoretical procedure to gain insights into the geometrical and electronic structures of the dyes, and (iii) to bring out the adequate structural modifications that will optimize the properties of the TPA-based DSSCs.

It is clear that, on the basis of the agreement with experimental data on these compounds, the BHandH hybrid is the functional of choice for the TDDFT calculations. Using this functional, the required accuracy for the design of new molecules is attained. Indeed, the mean average error is 9 nm/0.07 eV, in spite of the charge transfer nature of the excitations. This extremely satisfying accuracy results in part from the selection of quite extended basis sets and from the explicit consideration of bulk solvent effects. It is our experience that such effects are essential to reach a nice experiment/theory agreement.[78]

The electron injection efficiency to $TiO_2$ and the light harvesting abilities of the dyes have been investigated. Starting with the TPC-1 structure, the following modifications help to improve the properties of the DSSC: (i) an extension of the bridging group length by adding an ethylene between the two phenyl groups (TPC-14); (ii) the 16-COOH, 15-OMe, 1a,6-diCN functionalization (TPC-18); (iii) the displacement of the terminal −CN group from the position 16 to the 15, and the substitution of the hydrogen atoms by two -OMe functions in positions 11 and 13, as well as grafting two −CN groups in positions 1a and 6 of the TPA moiety (TPC-20). These changes induce a maximal increase of the LHE and provide a highly exoenergic free enthalpy of injection ($-2.20 \pm 0.45$ eV, compared to $-1.84 \pm 0.45$ eV for TPC-1). Following the MOA, we expect TPC-14 and TPC-20 have much better orbital overlap with the $TiO_2$ conduction band than dyes containing rhodanine-3-acetic acid (TPR-1) or dyes substituted by several EDGs on the dye tail (TPC-19). Finally, we considered two additional structures resulting from the "chemical addition" of TPC-14 and TPC-18 (to give TPC-22), and TPC-14 and TPC20 (to give TPC-23). The characterization of these two new compounds reveals that, compared to the three TPC-14, TPC-18, and TPC-20, only TPC-23 shows an improvement of both RLHE and $\Delta G_r^{inject}$ parameters. The examination of the atomic charges and molecular topology demonstrates that the positive charge is completely diluted in the conjugated bridging group. However, since the coplanarity between the −CHCN−CHCOOH anchoring part and the bridging unit is broken (∼60° out-of-plane distortion), the diluted positive charge is not directly in contact with the $TiO_2$ surface and the recombination reaction is therefore inhibited.

**Acknowledgment.** J.P., D.J., E.A.P., and C.M. thank the Belgian National Fund for Scientific Research (FRS-FNRS) for their respective positions. All calculations have been performed on the Interuniversity Scientific Computing Facility (ISCF), installed at the Facultés Universitaires Notre-Dame de la Paix (Namur, Belgium), for which the authors gratefully acknowledge the financial support of the FNRS-FRFC and the "Loterie Nationale" for the convention number 2.4578.02 and of the FUNDP.

## References and Notes

(1) Heimer, T. A.; Heilweil, E. J.; Bignozzi, C. A.; Meyer, G. J. *J. Phys. Chem. A* **2000**, *104*, 4256.
(2) Nazeeruddin, M. K. *Coord. Chem. Rev.* **2004**, *248*, 1161.
(3) Kamat, P. V.; Haria, M.; Hotchandani, S. *J. Phys. Chem. B* **2004**, *108*, 5166.
(4) Bisquert, J.; Cahen, D.; Hodes, G.; Ruehle, S.; Zaban, A. *J. Phys. Chem. B* **2004**, *108*, 8106.
(5) Furube, A.; Katoh, R.; Yoshihara, T.; Hara, K.; Murata, S.; Arakawa, H.; Tachiya, M. *J. Phys. Chem. B* **2004**, *108*, 12588.
(6) Li, G.; Jiang, K. J.; Li, Y. F.; Li, S. L.; Yang, L. M. *J. Phys. Chem. C* **2008**, *112*, 11591.
(7) Nazeeruddin, M. K.; De Angelis, F.; Fantacci, S.; Selloni, A.; Viscardi, G.; Liska, P.; Ito, S.; Bessho, T.; Grätzel, M. *J. Am. Chem. Soc.* **2005**, *127*, 16835.
(8) Wang, S. Z.; Cui, Y.; Hara, K.; Dan-Oh, Y.; Kasada, C.; Shinpo, A. *Adv. Mater.* **2007**, *19*, 1138.
(9) Sayama, K.; Hara, K.; Mori, N.; Satsuki, M.; Suga, S.; Tsukagochi, S.; Abe, Y.; Sugihara, H.; Arakawa, H. *Chem. Commun.* **2000**, 1173.
(10) Horiuchi, T.; Miura, H.; Sumioka, K.; Uchida, S. *J. Am. Chem. Soc.* **2004**, *126*, 12218.
(11) Hara, K.; Horiguchi, T.; Kinoshita, T.; Sayama, K.; Sugihara, H.; Arakawa, H. *Sol. Energy Mater. Sol. Cells* **2000**, *64*, 115.
(12) Stathatos, E.; Lianos, P.; Laschewsky, A.; Ouari, O.; Van Cleuvenbergen, P. *Chem. Mater.* **2001**, *13*, 3888.
(13) Ferrere, S.; Zaban, A.; Gregg, B. *J. Phys. Chem. B* **1997**, *101*, 4490.
(14) Ferrere, S.; Gregg, B. *New J. Chem.* **1997**, *26*, 1155.
(15) Liu, D.; Fessenden, R. W.; Hug, G. L.; Kamat, P. V. *J. Phys. Chem. B* **1997**, *101*, 2583.
(16) Burfeindt, B.; Hannappel, T.; Storck, W.; Willig, F. *J. Phys. Chem.* **1996**, *100*, 16463.
(17) Sayama, K.; Tsukagochi, S.; Hara, K.; Ohga, Y.; Shinpou, A.; Abe, Y.; Suga, S.; Arakawa, H. *J. Phys. Chem. B* **2002**, *106*, 1363.
(18) Ning, Z.; Zhang, Q.; Wu, W.; H., P.; Tian, H. *J. Org. Chem.* **2008**, *73*, 3791.
(19) Tian, H.; Yang, X.; Chen, R.; Zhang, R.; Hagfeldt, A.; Sun, L. *J. Phys. Chem. C* **2008**, *112*, 11023.
(20) Xu, W.; Peng, B.; Chen, J.; Liang, M.; Cai, F. *J. Phys. Chem. C* **2008**, *112*, 874.
(21) Lin, J. T.; Chen, P. C.; Yen, H. Y. C., Y. S.; Chou, H. H.; Yeh, M. C. P. *Org. Lett.* **2009**, *11*, 97.
(22) Jamorski-Jödicke, C.; Lüthi, H. P. *J. Am. Chem. Soc.* **2002**, *125*, 252.
(23) Jamorski-Jödicke, C.; Lüthi, H. P. *J. Chem. Phys.* **2002**, *117*, 4146.
(24) Preat, J.; Jacquemin, D.; Wathelet, V.; André, J. M.; Perpète, E. A. *J. Phys. Chem. A* **2006**, *110*, 8144.
(25) Cossi, M.; Barone, V. *J. Chem. Phys.* **2001**, *115*, 4708.
(26) Adamo, C.; Barone, V. *Chem. Phys. Lett.* **2000**, *330*, 152.
(27) Adam, W.; Krebs, O. *Chem. Rev.* **2003**, *103*, 4131.
(28) Baerends, E. J.; Ricciardi, G.; Rosa, A.; van Gisbergen, S. J. A. *Coord. Chem. Rev.* **2002**, *230*, 5.
(29) Jacquemin, D.; Preat, J.; Wathelet, V.; Fontaine, M.; Perpète, E. A. *J. Am. Chem. Soc.* **2006**, *128*, 2072.
(30) Tawada, T.; Tsuneda, T.; Yanagisawa, S.; Yanai, T.; Hirao, K. *J. Chem. Phys.* **2004**, *120*, 8425.
(31) Kamiya, M.; Sekino, H.; Tsuneda, T.; Hirao, K. *J. Chem. Phys.* **2005**, *122*, 234111.
(32) Chiba, M.; Tsuneda, T.; Hirao, K. *J. Chem. Phys.* **2006**, *124*, 144106.
(33) Jacquemin, D.; Perpète, E. A.; Scuseria, G.; Ciofini, I.; Adamo, C. *J. Chem. Theory. Comput.* **2008**, *4*, 123.
(34) Peach, M. J. G.; Benfield, P.; Helgaker, T.; Tozer, D. J. *J. Chem. Phys.* **2008**, *128*, 044118.
(35) Rohrdanz, M. A.; Herbert, J. M. *J. Chem. Phys.* **2008**, *129*, 034107.
(36) Guillaume, M.; Champagne, B.; Zutterman, F. *J. Phys. Chem. A* **2006**, *110*, 13007.
(37) Bertolino, C. A.; Ferrari, A. M.; Barolo, C.; Viscardi, G.; Caputo, S.; Coluccia, G. *Chem. Phys.* **2006**, *52*, 330.
(38) Prieto, J. B.; Arbeloa, F. L.; Martinez, V. M.; Arbeloa, I. L. *Chem. Phys.* **2003**, *13*, 296.
(39) Jacquemin, D.; Perpète, E. A.; Scalmani, G.; Frisch, M. J.; Kobayashi, R.; Adamo, C. *J. Chem. Phys.* **2007**, *126*, 144105.
(40) Amovilli, C.; Barone, V.; Cammi, R.; Cancès, E.; Cossi, M.; Mennucci, B.; Pomelli, C. S.; Tomasi, J. *Adv. Quantum Chem.* **1998**, *32*, 227.
(41) Tomasi, J.; Mennucci, B.; Cammi, R. *Chem. Rev.* **2005**, *105*, 2999.
(42) Frisch, M. J. *Gaussian DVP, Revision D.02*; Gaussian, Inc.: Wallingford, CT, 2005.
(43) Møller, C.; Plesset, M. S. *Phys. Rev.* **1934**, *46*, 618.
(44) Krishnan, R.; Binkley, J. S.; Seeger, R.; Pople, J. A. *J. Chem. Phys.* **1980**, *72*, 650.
(45) Becke, A. D. *J. Chem. Phys.* **1993**, *98*, 1372.
(46) Becke, A. D. *Phys. Rev. A* **1988**, *38*, 3098.
(47) Lee, C.; Yang, W.; Parr, R. G. *Phys. Rev. B* **1988**, *37*, 785.
(48) Becke, A. D. *J. Chem. Phys.* **1993**, *98*, 5648.
(49) Adamo, C.; Barone, V. *J. Chem. Phys.* **1999**, *110*, 6158.

(50) Ernzerhof, M.; Scuseria, G. E. *J. Chem. Phys.* **1999**, *110*, 5029.
(51) Perdew, J. P.; Burke, K.; Ernzerhof, M. *Phys. Rev. Lett.* **1996**, *77*, 3865.
(52) Perdew, J. P.; Ernzerhof, M.; Burke, K. *J. Chem. Phys.* **1996**, *105*, 9982.
(53) Handy, N. C.; Cohen, A. J. *Mol. Phys.* **2001**, *99*, 403.
(54) Naumov, V. A.; Samdal, S.; Naumov, A. V.; Gundersen, S.; Volden, H. V. *Russ. J. Gen. Chem.* **2005**, *75*, 1956.
(55) Guillaumont, D.; Nakamura, S. *Dyes Pigm.* **2000**, *46*, 85.
(56) Li, Q.; Zhang, X. X.; Meng, Y.; Chen, M. B. *Chin. Chem. Lett.* **2005**, *16*, 693.
(57) Magyar, R. J.; Tretiak, S. *J. Chem. Theory Comput.* **2007**, *3*, 976.
(58) Brédas, J. L.; Beljonne, D.; Coropceanu, V.; Cornil, J. *J. Chem. Rev.* **2004**, *104*, 4971.
(59) Preat, J.; Jacquemin, D.; Wathelet, V.; André, J. M.; Perpète, E. A. *Chem. Phys.* **2007**, *335*, 177.
(60) Loison, C.; Antoine, R.; Broyer, M.; Dugroud, J.; Guthmuller, J.; Simon, D. *Chem.—Eur. J.* **2008**, *14*, 7351.
(61) Improta, R.; Barone, V.; Scalmani, G.; Frisch, M. J. *J. Chem. Phys.* **2006**, *125*, 054103.
(62) Katoh, R.; Furube, A.; Yoshihara, T.; Hara, K.; Fujihashi, G.; Takano, S.; Murata, S.; Arakawa, H.; Tachiya, M. *J. Phys. Chem. B* **2004**, *108*, 4818.
(63) Asbury, J. B.; Wang, Y. Q.; Hao, E.; Ghosh, H.; Lian, T. *Res. Chem. Intermed.* **2001**, *27*, 393.
(64) Hagfeldt, A.; Grätzel, M. *Chem. Rev.* **1995**, *95*, 49.
(65) Cave, R. J.; Castner, E. W., Jr. *J. Phys. Chem. A* **2002**, *106*, 12117.
(66) Cave, R. J.; Burke, K.; Castner, E. W., Jr. *J. Phys. Chem. A* **2002**, *106*, 9294.
(67) Barbara, P. F.; Meyer, T. J.; Ratner, M. A. *J. Phys. Chem.* **1996**, *100*, 13148.
(68) Matthews, D.; Infelta, P.; Grätzel, M. *Sol. Energy Mater. Sol. Cells* **1996**, *44*, 119.
(69) Benkö, G.; Kallioien, J.; Korppi-Tommola, J. E. I.; Yartsev, A. P.; Sundström, V. *J. Am. Chem. Soc.* **2002**, *124*, 489.
(70) Iwa, S.; Hara, K.; Murata, S.; Katoh, R.; Sugihara, H.; Arakawa, H. *J. Chem. Phys.* **2000**, *113*, 3366.
(71) Bauer, C.; Boschloo, G.; Mukhtar, E.; Hagfeldt, A. *Int. J. Photochem.* **2002**, *4*, 17.
(72) Cahen, D.; Hodes, G.; Grätzel, M.; Guillermoles, J. F.; Riess, I. *J. Phys. Chem. B* **2000**, *104*, 2053.
(73) Nalwa, H. S. *Handbook of Advanced Electronic and Photonic Materials and Devices*; Academic: San Diego, 2001.
(74) Hagberg, D. P.; Marinado, T.; Karlsson, K. M.; Nonomura, K.; Qin, P.; Boschloo, G.; Brinck, T.; Hagfeldt, A.; Sun, L. *J. Org. Chem.* **2007**, *72*, 9550.
(75) Chen, R.; Yang, X.; Tian, H.; Wang, X.; Hagfeldt, A.; Sun, L. *Chem. Mater.* **2007**, *19*, 4007.
(76) Hagfeldt, A.; Grätzel, M. *Acc. Chem. Res.* **2000**, *33*, 269.
(77) Besler, B. H.; Merz, K. M.; Kollman, P. A. *J. Comput. Chem.* **1990**, *11*, 431.
(78) Jacquemin, D.; Perpète, E. A.; Ciofini, I.; Adamo, C. *Acc. Chem. Res.* **2009**, *42*, 326.

JP904946A